ISSN: 1231-4005
e-ISSN: 2354-0133
DOI: 10.5604/12314005.1138363

NUMERICAL MODELLING AND VALIDATION OF 12.7 MM FSP IMPACT INTO ALFC SHIELD – ARMOX 500T STEEL PLATE SYSTEM

Marian Klasztorny, Marek Świerczewski

Military University of Technology
Department of Mechanics and Applied Computer Science
Gen. S. Kaliski Street 2, 00-908 Warsaw, Poland
tel.: +48 22 6839947, fax: +48 22 6839355
e-mail: mklasztorny@wat.edu.pl, mswierczewski@wat.edu.pl

Abstract

The study develops a methodology for numerical modelling and simulation of a 12.7 mm 13.4 g FSP fragment impact into the ALFC shield – ARMOX 500T steel plate system. The ALFC shield is composed of the ALF energy-absorbing subsystem and a 10 mm-thick 99,7% Al_2O_3 alumina ceramic layer. The ALF subsystem is designed to absorb blast wave impact energy induced by explosive materials up to 10 kg TNT. The ceramic layer is designed to stop fragments from IED explosion. The 5 mm-thick Armox 500T steel plate constitutes the body bottom segment of a light armoured vehicle. The ALF subsystem has the following layered structure: Al2024 aluminium alloy plate, SCACS hybrid laminate plate, ALPORAS aluminium foam, SCACS hybrid laminate plate. The layers are joined with Soudaseal 2K chemoset glue. SCACS hybrid laminate contains the following components: VE 11-M modified vinylester resin (matrix), SWR800 S-glass plain weave fabric, Tenax HTA40 6K carbon plain weave fabric, Kevlar 49 T 968 aramid plain weave fabric. The total thickness of the ALFC shield amounts to 90 mm. Proof ground tests of a 12.7 mm 13.4 g FSP fragment impact into the ALFC shield – ARMOX 500T steel plate system have been performed at impact velocity 715 m/s and used for experimental validation of numerical modelling and simulation. In the numerical modelling, the aluminium alloy plate and Armox 500T steel plate are working in the elasto-plastic range according to Johnson–Cook model. The 99.7% Al_2O_3 alumina ceramic is working in elasto-short range according to JH-2 Johnson–Holmquist model. The simulations correspond to large displacements, large deformations and potential contact among all the components of the system. In FE mesh, the 8-node 24 DOF hexahedral finite elements with single integration point have been used. Failure criteria governing ad-hoc erosion of finite elements have been applied. The FEM modelling, simulation and postprocessing have been carried out using Catia, HyperMesh, LS-DYNA and LS-PrePost systems. The simulation results in the form of displacement/penetration contours and the FSP final deformation have been compared with the experimental results.

Keywords*: light armoured vehicles, passive protection, IED, FSP, numerical modelling, simulation, validation*

1. Introduction

During peace-keeping military operations logistic (LV) and light-armoured vehicles (LAV) are exposed to blast of AT mines and IED devices (code AT–IED). The latter, apart from blast of explosive material, induce a high–velocity (1400–1800 m/s) stream of arbitrary shaped fragments, e.g. bearing balls, nails, bolts etc., which are capable of perforation the vehicle body shell and wounding/killing the occupants. Nowadays, the military research centres are designing new types of protective shields against AT-IED charges, which have the following features:

- high specific energy of AT/IED blast wave absorption through various failure mechanisms of the energy-absorbing layers,
- protection of the vehicle bottom from destruction/perforation induced by AT/IED explosion,
- keeping to a minimum plastic deformations of the vehicle body,
- limitation of AT/IED explosion-induced accelerations and forces, acting on the occupants, to the admissible levels from occupants' health/life point of view.

A new anti-AT/IED protective shield ALF applicable to protect LV/LAV vehicles up to 10 kg of TNT was designed and preliminary tested in [6, 7]. The shield contains the following energy-

absorbing – resistant layers (from the explosion side): the Al2024 aluminium plate, the SCACS hybrid laminate, the ALPORAS aluminium foam core, the SCACS hybrid laminate. The layers of ALF segments are integrated with glue joints using Soudaseal 2K chemoset glue. The SCACS hybrid laminate, manufactured using the RTM vacuum technology, contains the following uniform laminates: S – glass laminate, C – carbon laminate, and A – aramid laminate. The matrix constitutes incombustible VE 11-M vinylester resin. The reinforcement has been performed with plain weave fabrics: SWR800 S-glass fabric (substance 800 g/m^2), Tenax HTA40 6K carbon fabric (substance 300 g/m^2), Kevlar 49 T 968 aramid fabric (substance 230 g/m^2). The ALF shield has modular structure, 76 mm thickness, substance 50 kg/m^2. It is characterized by a relatively simple manufacturing, assembly and disassembly technology, long durability and relatively low material-manufacturing costs. The experimental and numerical preliminary investigations presented in [6, 7] constitute the basis to assess the ALF shields protection against AT/IED blast wave on level 3b according to standard [11]. On the other hand, the ALF shield does not protect LAVs from IED fragmentation according with requirements set up in [1]. Thus, an additional ultra-hard layer should be applied.

The study develops the ALFC protective system for total anti-AT/IED protection of LAV vehicles. The ALFC shield has layered structure and is composed of the ALF shield and the 99.7% Al_2O_3 alumina ceramic layer (layer C). There is considered the FSP–ALFC–PP system composed of a 12.7 mm 13.4 g FSP moving at impact velocity of 715 km/h, the ALFC shield and the 5 mm Armox 500T steel plate (layer PP). The main layers are joined with 2 mm Soudaseal 2K glue. The FSP standard fragment hits into the shield centrally and perpendicularly to the external surface. The main purpose of the study is to develop numerical modelling and simulation methodology and experimental validation of modelling and simulation of the FSP–ALFC–PP system.

2. Literature review

NATO documents [1, 2, 11, 12] formulate the requirements in reference to the occupants' protection against ballistic, artillery, and AT mine threats. However, these references do not formulate requirements in reference to IEDs. FSP (Fragment-Simulating Projectile) standard fragments of 12.7 mm 13.4 g and 20 mm 54 g types are defined in [1]. Proposals related to standardization of IED fragmentation resistance have been developed in [3, 5]. The IED fragmentation micro-range test has been proposed in [3] with the use of 20 mm 54 g FSP standard fragment compatible with [1, 11]. The writers assumed the multi-hit mode (6 series with 3 shots each) and the single-hit mode (12 one-by-one shots) for the tested protective shield – protected plate segment. Reference [3] does not formulate protection levels of LAV's crew-occupants against IED blast and fragmentation. Only the maximum lever is proposed, corresponding to 155 mm M107 artillery missile blast under the vehicle.

Range tests on 155 mm M107 artillery missile explosion and fragmentation, used to simulate IED, are described in [5]. Mass distribution as well as geometry and velocity of the fragments have been determined.

Numerical modelling of the 0.22 in 17 grains FSP (5.46 mm 1.14 g FSP) impact into 100×100 mm two-layer plate (aramid composite, steel) has been developed in [10]. This is the standard fragment in ballistic tests for missile resistant jackets and helmets [8]. The material constants have been taken from [13]. The simulations have been conducted using FE code LS-Dyna. The FSP was modelled as a rigid body, whereas the plate was discretized using 4-node shell elements. The writers considered two impact velocities, i.e. 500 m/s (1800 km/h) and 1000 m/s (3600 km/h); in both cases the protected plated has been perforated.

3. Micro-range tests of the FSP–ALFC–PP system

Perforation tests for the FSP–ALFC–PP system have been conducted in 2010 in Military Institute of Armour and Vehicle Technology, Zielonka, Poland. The ALFC segment of overall

dimensions 200×200×95 mm was fixed in the rigid vertical steel frame. The impact and penetration process was registered with Phantom V12 high-speed video camera.

Figure 1 presents the ALFC specimen after the test performed according to the multi–hit mode impacting specification given in Ref. [3]. The impact velocities amounted to: shot #1: 698 m/s, shot #2: 715 m/s, shot #3: 732 m/s. Shot #2 has been selected for the validation process.

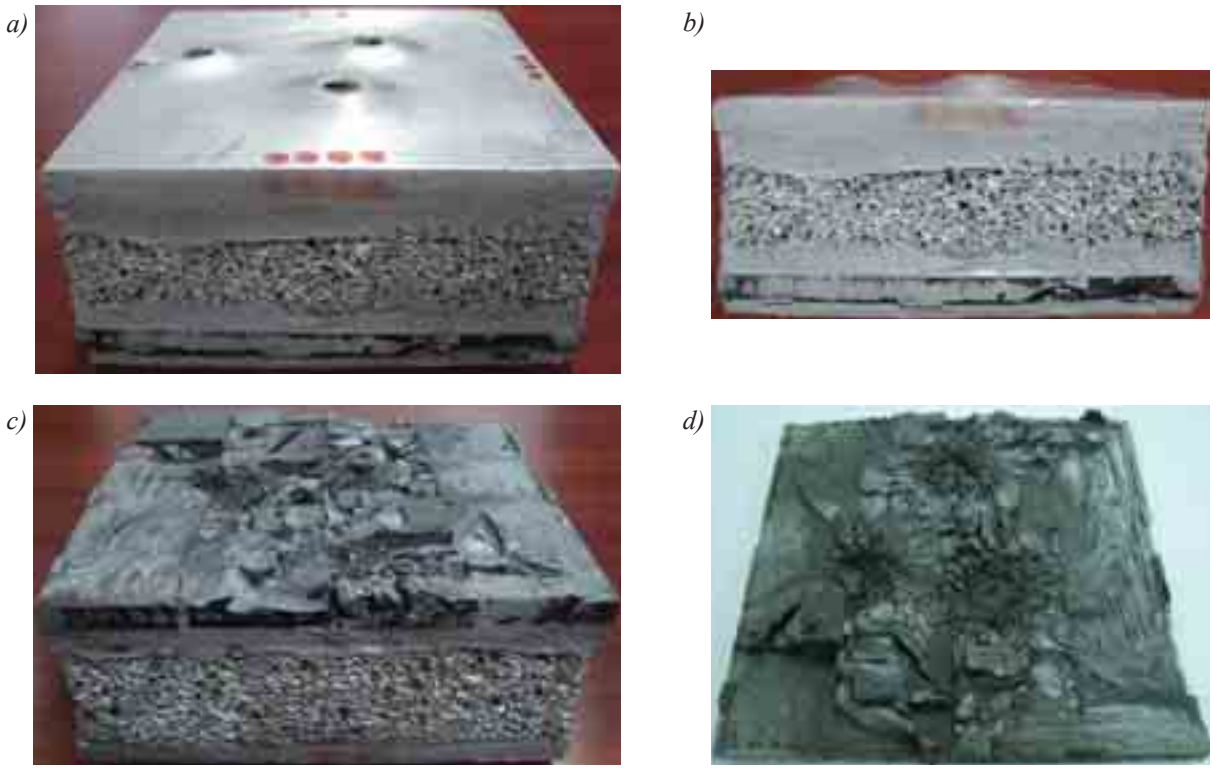

Fig. 1. The ALFC shield specimen after the 12.7 mm 13.4 g FSP impact tests: a) an axonometric view on the craters in the aluminium sheet; b) a side view on the specimen; c) an axonometric view on the damaged ceramic layer after separation of the protected plate; d) an axonometric view on the protected plated with glued ceramic elements

The conclusions resulting from the experimental tests are formulated below:

1) Each shot had not caused perforation of the ALFC – protected plate system. The fragments have been stopped in the ceramic layer close to the one-third thickness of this layer. The fragments have been deformed plastically.
2) There had formed small craters on the front (Al2024 aluminium alloy) side of the specimen.
3) The ALF structural layers (laminates, foam, glue) had eroded cylindrically along with each shot line.
4) Integrity of the ALFCC–PP specimens has been kept. Only intensive cracks in the central area of the ceramic layer have been occurred.
5) The ALFC shield protects the PP plate against perforation or even plastic deformation induced by impact of a 12.7 mm 13.4 g FSP moving at 715 m/s impact velocity.

The FSP fragment corresponding to shot #2 has been photographed and measured before and after the test. The results are presented in further considerations.

4. Numerical modelling and simulation of FSP impact into ALFC–PP system

Taking into consideration the conclusions resulting from the validation impact test (see chapter 3), the overall dimensions of the ALFC–PP specimen have been decreased to 120×120×95 mm^3 in order to simulate a single impact. The specimen was hit centrally and perpendicularly to the front aluminium plate by a 12.7 mm 13.4 g FSP at 715 m/s impact velocity. The ALFC–PP specimen is

fixed in the rigid vertical steel frame in the way analogical to the experimental test described in Section 3. Thicknesses of subsequent structural energy-absorbing – resistant layers in the ALFC shield amount to:

– aluminium sheet (Al2024 alloy): 2 mm,
– SCACS hybrid laminate: 9 mm,
– ALPORAS aluminium foam: 50 mm,
– SCACS hybrid laminate: 9 mm.
– 99.7% Al_2O_3 alumina ceramics: 10 mm.

The glue layers integrating the structural layers in one brick have thickness 2 mm.

An FSP fragment is made of 4340H cold-rolled annealed alloy steel of 30±2 HRC hardness or equivalent (e.g. 4337H, 4340H types) [1, 3].

A concept of numerical modelling and simulation of 12.7 mm 13.4 g FSP at impact velocity 715 m/s into the ALFC–PP subsystem is described below:

1) The external aluminium plate and the protected plate (Armox 500T steel) are working in the nonlinear elasto-plastic range taking into account high strain rates (Johnson–Cook model) [4]. The plates are exposed to large displacements and large plastic deformations.
2) The 99.7% Al_2O_3 ceramics is treated as the nonlinear elasto-short material taking into account high strain rates (Johnson–Holmquist model) [4].
3) The uniform laminates (S – glass, C – carbon, A – aramid reinforced plastics), ALPORAS aluminium foam, and Soudaseal 2K glue are described by respective models not taking into account high strain rates. All possible failure mechanisms for these materials as well as large displacements and large deformations are taken into consideration.
4) Possible contact among all the components and dry friction between the ALFC–PP subsystem and the steel frame are taken into account. The contact was modelled using AUTOMATIC_SINGLE_SURFACE and SEGMENT_BASED_CONTACT (SOFT 2) options [4].
5) The influence of air and gravitation are neglected.
6) Owing to bisymmetry of the system, the FE model has been limited to a quarter of the system. The central zone is meshed with high density whereas the extracentral zone is meshed with medium density (Fig. 7). In the area contact of the dense and rare meshes the CONTACT_TIED_NODES_TO_SURFACE_OFFSET option has been applied [4].
7) The 8-nodes brick finite elements, with 24 DOFs and one integration point, were used taking into account contact and friction phenomena. The FE models are relatively dense and finite elements' dimensions satisfy the aspect ratio requirements before and during the impact and penetration process. Six types of hourglass control were included.
8) The initial-boundary conditions contain the vertical impact velocity of the FSP fragment, fastening of the impacted ALFC–PP subsystem in the horizontal rigid steel frame realized as contact of the subsystem with the horizontal rigid walls, description of interaction between the components realized as the penalty rule contact (the contact stiffness was scaled with respect to the mass) and declaration of two vertical planes of symmetry.

The FE modelling, simulations and postprocessing have been performed using the following CAE systems: Catia (creating the geometrical models), Altair HyperMesh (automatic FE meshing), LS-PrePost (a pre-processor for defining all necessary parameters such as boundary conditions, element properties, material properties, the analysis type), LS-DYNA (a solver). The complete FE model was exported as a key file with LS-DYNA preferences. The Lagrangian domain was limited by two planes of symmetry of the system to reduce CPU time. In the simulations the LS-DYNA nonlinear explicit code was used.

Figure 2 presents the numerical model of the FSP–ALFC–PP system quarter. The extracentral zone in ALFC–PP subsystem the was meshed analogically as in [6], whereas in the central zone FE mesh is denser 4 times in aluminium and steel plates and 2 times in the remaining layers compared to the rare mesh. The total number of finite elements amounts to more than 230 000. The FSP fragment mesh contains more than 4000 FEs.

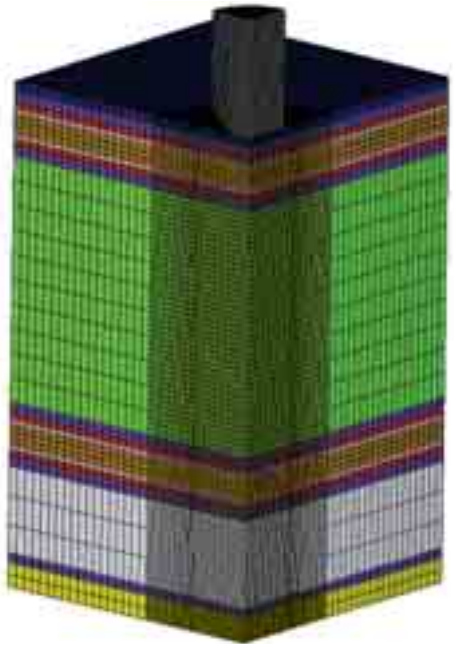

Fig. 2. The numerical model of the FSP–ALFC–PP system (an axonometric view)

For Armox 500T steel, 4340 steel, and Al2024 aluminium alloy LS-DYNA material type MAT_15 (MAT_JOHNSON_COOK), EOS_GRUNEISEN equation-of-state and JC failure model have been assumed [4].

For plain weave fabric reinforced uniform laminates LS-Dyna material type MAT_161 (MAT_ COMPOSITE_MSC) has been chosen, [4]. This model is addressed to layered composites reinforced with two-directional fabrics. The model reflects the progressive failure criteria, including delamination. The failure criteria have been established by adopting the methodology developed by Hashin. The SCACS hybrid laminate is a sequence of uniform laminates S, C, A, C, S modelled as linear elasto-short orthotropic materials after homogenization. The ply sequence in the SCACS laminate is $[(0/90)_S]_2$, $[(0/90)_C]_4$, $[(0/90)_A]_{12}$, $[(0/90)_C]_4$, $[(0/90)_S]_2$.

For ALPORAS aluminium foam LS-DYNA material type MAT_026 (MAT_HONEYCOMB) has been selected. This material model is useful for honeycomb and foam materials. A nonlinear elasto-plastic behaviour is defined separately for all normal and shear stresses considered to be fully uncoupled. After homogenization, ALPORAS foam is modelled as an orthotropic material with its mechanical properties identical in three orthogonal directions. The elastic moduli vary from the initial non-compacted values to the fully compacted values. The normal stress vs. volumetric strain and the shear stress vs. volumetric strain load curves are required in this model. The proportionality coefficient of these curves equals 0.50 and has been derived from the additional validation test.

For SOUDASEAL 2K glue LS-Dyna material type MAT_027 (MAT_MOONEY_RIVLIN_ RUBBER) has been assumed. This is a two-parametric material model for rubber. The axial force vs. actual change in the gauge length in the uniaxial tension test is required in the material data card [4].

For 99.7% Al_2O_3 corundum ceramics LS-DYNA material type MAT_110 (MAT_JOHNSON_ HOLMQUIST_CERAMICS) has been applied. The equation-of-state in the polynomial form without the thermal component and JH-2 failure model have been selected, [4].

The material constants for 4340 steel (FSP fragment) and 99.7% Al_2O_3 corundum ceramics are set up in Tab. 1 and 2. The material constants for the remaining materials used in the ALFC–PP subsystem are given in [6].

The erosion criteria have been set up with MAT_ADD_EROSION card taking into consideration the ultimate strains at failure, i.e. effective strains EFFEPS, bulk strains VOLEPS, and shear strains ESPPH. Assumed values, based on [9], are collected in Tab. 3 where DMGEXP is the exponent for the nonlinear damage accumulation.

Tab. 1. Material data for 4340 steel, [4, 9]

Parameter	Unit	4340 steel
Mass density, RO	kg/mm^3	7.85E–6
Shear modulus, G	GPa	79.6
Formulation for rate effects: scale yield stress, VP	–	0
Input constants for the flow stress: A	GPa	0.792
B	GPa	0.510
N	–	0.260
C	–	0.014
M	–	1.030
Melt temperature, TM	K	1800
Room temperature, TR	K	293
Quasi-static threshold strain rate, EPSO	1/ms	0.001
Specific heat, CP	J/(kg·K)	450
Spall type, SPALL	–	2
Plastic strain iteration option: accurate iterative solution, IT	–	1
Failure parameters: D1, D2, D3, D4, D5	–	0, 0, 0, 0, 0
Intercept, C	m/s	–
Slope coefficients: S1, S2, S3	–	–, 0, 0
Gruneisen gamma, GAMAO	–	–
First order volume correction, A	–	–

Tab. 2. Material constants for 99.7% Al_2O_3 corundum ceramics, [4, 9]

Parameter	Unit	Value
Density, RO	kg/mm^3	3.89E–6
Shear modulus, G	GPa	152.0
Material constants for JH-2 model:		
– Intact normalized strength parameter, A	–	0.88
– Fractured normalized strength parameter, B	–	0.45
– Strength parameter (for strain rate dependence), C	–	0.007
– Fractured strength parameter (pressure exponent), M	–	0.60
– Intact strength parameter (pressure exponent), N	–	0.64
Maximum tensile pressure strength, T	GPa	0.462
Hugoniot elastic limit, HEL	GPa	7.0
Fraction of elastic energy loss converted to hydrostatic energy (affects bulking pressure that accompanies damage), BETA	–	1
Maximum normalized fractured strength, SFMAX	–	1
Reference strain rate, EPSI	1/ms	0.001
Coefficients in the equation-of-state: K1, K2, K3	GPa	231, –160, 2774
Parameters in the failure model: D1, D2, FS	–	0.0125, 0.7, 0.0

Tab. 3. Parameters defining ad-hoc erosion of FEs, [9]

Component	EFFEPS	VOLEPS	EPSSH	DMGEXP
ALPORAS	0	0.05	0.5	1
S laminate	0	0.05	1	1
C laminate	0	0.05	1	1
A laminate	0	0.05	1	1
ARMOX 500 T	0	0.05	1	1
Al 2024	0	0.05	1	1
Soudaseal 2K	0.5	0.1	0.5	1
4340 steel	0	0.05	1	1
99.7% Al_2O_3 ceramics	0	0.05	1	1

5. The numerical simulations and the results

The computations have been conducted at Department of Mechanics and Applied Computer Science, Military University of Technology, Warsaw, Poland using FE code LS-Dyna v971. The simulation results are obtained in the form of total displacement contours illustrating the impact and penetration process (Fig. 3) and of the FSP kinetic energy diagram vs. time (Fig. 4). The 12.7 mm 13.4 FSP fragment penetrates all energy-absorbing – resistant layers and stops inside the ceramic layer (ca. at 2/3 ceramics thickness). The plastic deformation of the FSP fragment after the impact test will be shown in the next Section.

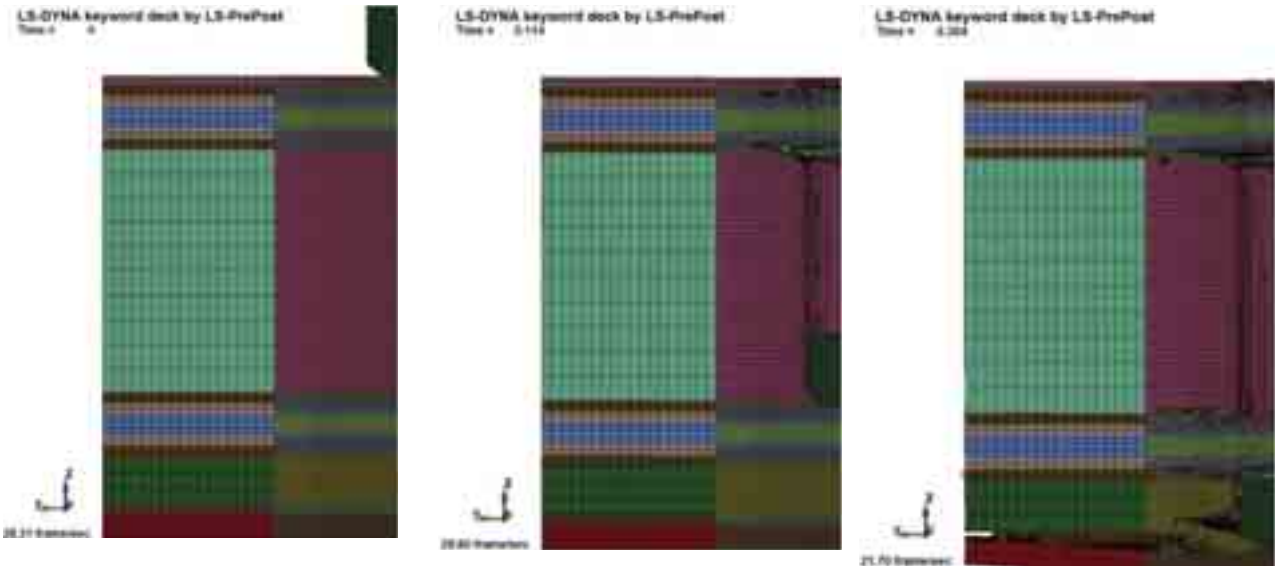

Fig. 3. The total displacement contours of the FSP–ALFC–PP system (the side views at the vertical cross-section coinciding the symmetry plane) at selected time points, for 10 mm thick ceramic layer, illustrating the impact and perforation process

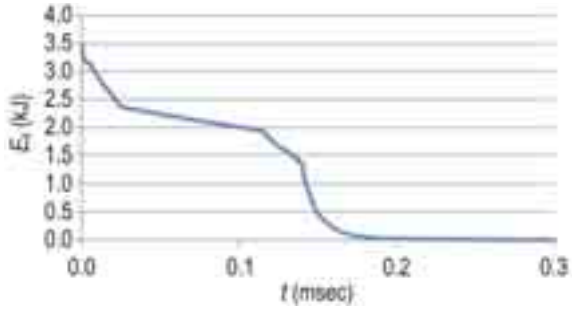

Fig. 4. The kinetic energy diagram for 12.7 mm 13.4 g FSP vs. time

6. Experimental validation of the numerical modelling and simulation

Experimental validation is aimed at verification of correctness of the numerical modelling and simulation methodology in reference to 12.7 mm 13.4 g FSP impact into the ALFC–PP subsystem. The validation criterion has been defined as conformability, both qualitative and quantitative, of the simulated and the experimental FSP plastic deformation after the impact and perforation test. Moreover, the total displacement contour has been compared to the experimental specimen after the test.

Figure 5 shows the 12.7 mm 13.4 g FSP fragment in the experiment test and in the simulated test, before and after the impact test. Tab. 4 collects the overall dimensions of the fragment before and after the impact test detected in the experimental and the simulated test. The following notation has been incorporated:

d_{ot}, d_{ob}, h_o – the top diameter, the bottom diameter, length of the FSP before the test,
d_t, d_b, h – the top diameter, the bottom diameter, length of the FSP after the test.

Based on Fig. 5 and Tab. 4, conformability, both qualitative and quantitative, of the FSP plastic deformation has been assessed as satisfactory.

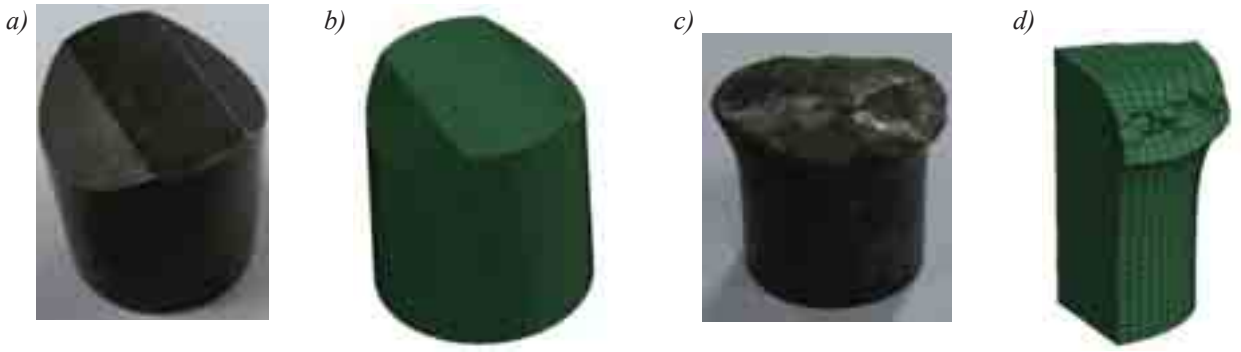

Fig. 5. The 12.7 mm 13.4 g FSP fragment and its numerical model before and after the impact and penetration test: a) the real fragment before the test, b) the numerical fragment before the test, c) the real fragment after the test, d) the numerical fragment quarter after the test (bisymmetry)

Tab. 4. The overall dimensions of the 12.7 mm 13.4 g FSP fragment before and after the impact and penetration test

Dimension	Value [mm]	
	experimental (average)	simulated
d_{ot}	12.60	12.60
d_t	14.53	14.73
d_{ob}	12.60	12.60
d_b	12.48	12.56
h_o	14.40	14.40
h	13.15	12.65

Figure 6 illustrates the final form of deformation and penetration in the FSP–ALFC–PP system at the central vertical cross-section of the system. Taking into account Fig. 1 and 5, conformability of the simulated test and the experimental test is acceptable.

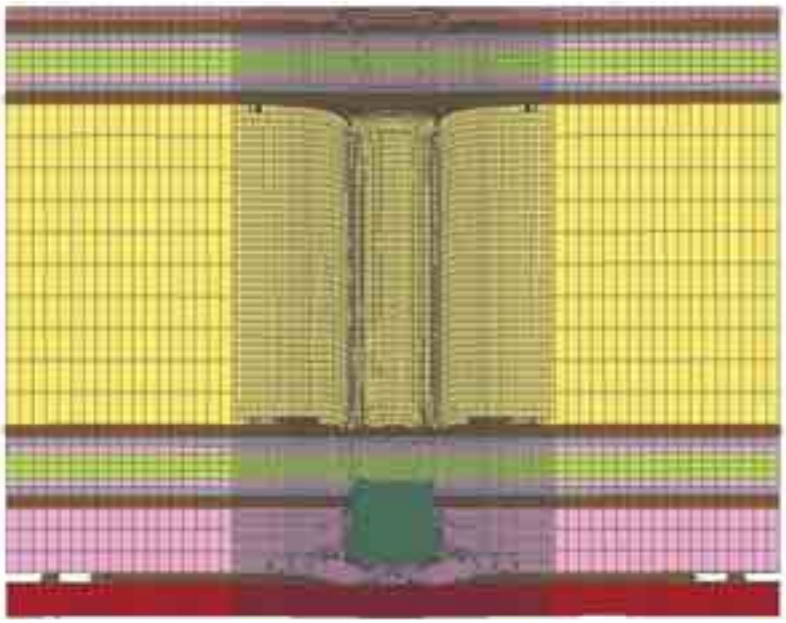

Fig. 6. The final total deformation and penetration in the FSP–ALFC–PP system

7. Final conclusions

The study develops the original ALFC shield for protection of light armoured vehicles against AT–IED blasts. The vehicle body shell bottom is in the form of a 5 mm ARMOX 500T steel plate.

The 12.7 mm 13.4 g FSP fragment moving at 715 m/s impact velocity creates a slight crater in the external aluminium sheet and the quasi-cylindrical hole enclosing all structural energy-absorbing – resistant layers in the ALFC shield. The fragment has stopped at ca. 2/3 thickness of the ceramic layer.

The fragment is due to small erosion during the penetration process. The simulated final plastic deformation of the FSP fragment is close to the experimental data. The plastic deformations in the protected plate are negligible.

The FSP kinetic energy diagram confirms high energy-absorption of the ALFC shield and full protection from perforation of the 5 mm Armox 500T plate (reflecting the vehicle bottom plate) induced by a 12.7 mm 13.4 g FSP fragment moving at 715 m/s impact velocity.

The numerical modelling and simulation of the FSP–ALFC–PP system has been validated positively.

References

[1] *AEP-55, Volume 1 (Ed. 1): Procedures for Evaluating the Protection Levels of Logistic and Light Armoured Vehicles for KE and Artillery Threats*, NATO/PFP Unclassified.

[2] *AEP-55, Volume 2 (Ed. 1): Procedures for Evaluating the Protection Levels of Logistic and Light Armoured Vehicle Occupants for Grenade and Blast Mine Threats Level*, NATO/PFP Unclassified.

[3] *DGLEPM DGLEPM T & E Engineering Std. – Improvised Explosive Device Protection Systems*, LOI/P&A for TAPV Project, Unclassified.

[4] Hallquist, J. O. (Ed.), *LS-DYNA V971 R4 Beta. Keyword User's Manual*, LSTC Co., CA, USA 2009.

[5] Karpenko, A., Ceh, M., *Experimental Simulation of Fragmentation Effects of an Improvised Explosive Device*, 23rd International Symposium on Ballistics, Tarragona, Spain 2007.

[6] Klasztorny, M., Dziewulski, P., Niezgoda, T., Morka, A., *Modelling and Numerical Simulation of the Protective Shield – Protected Plate – Test Stand System Under Blast Shock Wave*, Journal of KONES Powertrain and Transport, Vol. 17, No. 3, pp. 197-204, 2010.

[7] Klasztorny, M., Niezgoda, T., Panowicz, R., Gotowicki, P., *Experimental Investigations of the Protective Shield – Protected Plate – Test Stand System Under Blast Shock Wave*, Journal of KONES Powertrain and Transport, Vol. 17, No. 4, pp. 229-236, 2010.

[8] *MIL-DTL-46593B (MR), Detail Specification. Projectile, Calibres .22, .30, .50 and 20 mm Fragment-Simulating*, Department of Defense, USA 2008.

[9] Morka, A., *Material Data Basis* [in Polish], Research Report [unpublished], Military University of Technology, Warsaw, Poland 2010.

[10] Niezgoda, T., Kosiuczenko, K., Barnat, W., Panowicz, R., *Numerical Analysis of Impact of the Fragment into the Layered Plate*, Open-Cast Mining [Górnictwo Odkrywkowe], Vol. 59, No. 3, pp. 61-64, 2010.

[11] *STANAG 4569 (Ed. 1): Protection Levels for Occupants of Logistic and Light Armoured Vehicles*, NATO/PFP Unclassified.

[12] *STANAG 4190: Test Procedures for Measuring Behind-Armour Effects of Anti-Armour Ammunition*, NATO/PFP Unclassified.

[13] Tham, C. Y., Tan, V. B. C., Lee, H. P., *Ballistic Impact of a Kevlar Helmet. Experiment and Simulations*, International Journal of Impact Engineering, Vol. 35, No. 5, pp. 304-318, 2008.